IOPscience iopscience.iop.org

Home Search Collections Journals About Contact us My IOPscience

Multi-frequency orthogonality sampling for inverse obstacle scattering problems

This article has been downloaded from IOPscience. Please scroll down to see the full text article.

2011 Inverse Problems 27 085005

(http://iopscience.iop.org/0266-5611/27/8/085005)

View the table of contents for this issue, or go to the journal homepage for more

Download details:
IP Address: 139.18.6.246
The article was downloaded on 05/06/2013 at 21:15

Please note that terms and conditions apply.

IOP PUBLISHING INVERSE PROBLEMS

Inverse Problems **27** (2011) 085005 (23pp) doi:10.1088/0266-5611/27/8/085005

Multi-frequency orthogonality sampling for inverse obstacle scattering problems

Roland Griesmaier

Institut für Mathematik, Johannes Gutenberg-Universität Mainz, Germany

E-mail: griesmai@uni-mainz.de

Received 18 February 2011, in final form 7 June 2011
Published 13 July 2011
Online at stacks.iop.org/IP/27/085005

Abstract

We discuss a simple non-iterative method to reconstruct the support of a collection of obstacles from the measurements of far-field patterns of acoustic or electromagnetic waves corresponding to plane-wave incident fields with one or few incident directions at several frequencies. The method is a variant of the orthogonality sampling algorithm recently studied by Potthast (2010 *Inverse Problems* **26** 074015). Our theoretical analysis of the algorithm relies on an asymptotic expansion of the far-field pattern of the scattered field as the size of the scatterers tends to zero with respect to the wavelength of the incident field that holds not only at a single frequency, but also across appropriate frequency bands. This expansion suggests some modifications to the original orthogonality sampling algorithm and yields a theoretical motivation for its multi-frequency version. We illustrate the performance of the reconstruction method by numerical examples.

(Some figures in this article are in colour only in the electronic version)

1. Introduction

Non-iterative reconstruction methods for inverse obstacle scattering problems for time harmonic acoustic or electromagnetic waves attracted a lot of interest in recent years and many innovative algorithms have been developed. Examples include the linear sampling method by Colton and Kirsch [11], the factorization method by Kirsch [24], the MUSIC-algorithm (see, e.g., Devaney [15], Ammari *et al* [4], Cheney [10], or Kirsch [25]), the probe method or the method of singular sources by Potthast [32], Ikehata's enclosure method [20], or the range test by Potthast *et al* [34], to name just a few. So far most of these methods use measurements of scattered fields at a single frequency as input data to recover information on the unknown scatterers. Few extensions exist to multi-frequency data (see, e.g., Guzina *et al* [17] for a linear sampling method or Luke [31] for a point-source method) or time-dependent measurements (see, e.g., Burkhard and Potthast [8] and Daido *et al* [14] for probe methods, Chen *et al* [9] for a linear sampling method, or Ikehata [21] for an enclosure method). In this

 © 2011 IOP Publishing Ltd Printed in the UK & the USA

paper we study a simple non-iterative reconstruction method for inverse obstacle scattering problems that process multi-frequency information. More precisely, the input data of this method are far-field patterns of scattered fields corresponding to plane-wave incident fields with one or few incident directions and several wave numbers. This algorithm is a variant of the orthogonality sampling method discussed by Potthast in [33]. The idea of orthogonality sampling is to evaluate a certain functional on a search domain that is to be scanned for scatterers. This functional is defined as a superposition of scalar products of far-field patterns of scattered waves with suitably chosen plane waves, such that it has large values close to scatterers and relatively small values otherwise. Its single frequency version is closely related to the back propagation algorithm for inverse scattering problems in bounded domains studied by Ammari [2, p 162], the stationary waves method by Vänskä [37], and the beam forming algorithm considered by Simonetti and Huang [35]. In contrast to the stationary waves method and beam forming, orthogonality sampling only requires the knowledge of far-field patterns corresponding to one or few incident directions of the incident field.

The theoretical foundation of the orthogonality sampling method is far less well developed than for the other qualitative reconstruction methods mentioned before. Our discussion of the method in this paper is based on an asymptotic analysis of the far-field pattern of the scattered field as the size of the scatterers becomes small with respect to the wavelength. Such expansions have been widely studied for penetrable obstacles and at fixed frequency of the incident field (see, e.g., Ammari *et al* [5], Ammari and Kang [7], Il'in [22], Jones [23], or Vogelius and Volkov [38]). Since we apply these formulas to justify a multi-frequency reconstruction method, we first have to show that the asymptotic expansions are valid not only for fixed frequencies, but also across a whole frequency band, as long as the scatterers are small with respect to the corresponding wavelengths. In doing so, we give a new short and concise proof of the expansions for sound soft scatterers, sound hard scatterers, and scatterers carrying an impedance boundary condition—three cases that have not been considered in detail so far—tracking explicitly their dependence on the wave number of the incident field. For a related discussion of uniform asymptotic expansions of the scattered field due to penetrable obstacles, we refer to Hansen and Vogelius [19].

The asymptotic analysis of the far-field patterns suggests some modifications to the original orthogonality sampling method, as studied in [33]. To compensate for the change in magnitude of the far-field pattern with increasing frequency we suggest to renormalize the input data depending on the material properties of the scatterers that we assume to be known. Furthermore, we incorporate an additional frequency-dependent phase shift in our reconstruction scheme. Therewith, the indicator function of the reconstruction method at a fixed frequency can be interpreted as the zeroth order Fourier coefficient of the far-field pattern of the scattered field in a suitably translated coordinate system. Applying classical results on integrals of Bessel functions this is used to establish a theoretical foundation of the multi-frequency version of the orthogonality sampling algorithm for small scatterers.

The paper is organized as follows. After introducing our notation as well as the direct and inverse scattering problem in the next section, we establish the uniform asymptotic expansions of the far-field pattern in section 3. Then, in section 4 we discuss the reconstruction algorithm. We comment on its numerical implementation and present numerical results in section 5. Finally, we draw some conclusions.

2. The mathematical setting

The following discussion is limited to scattering of time-harmonic waves due to impenetrable objects embedded in an unbounded two-dimensional homogeneous medium. Suppose

$D_1, \ldots, D_L \subset \mathbb{R}^2$ is a family of well-separated bounded domains with connected complement such that ∂D_l, $1 \leqslant l \leqslant L$, is of class C^2. Henceforth, we call $D_1, \ldots, D_L$ the scatterers and write $D := \bigcup_{l=1}^{L} D_l$ for the collection of all scatterers. We denote by

$$u^i(x; d, k) := \mathrm{e}^{\mathrm{i}kx\cdot d}, \qquad x \in \mathbb{R}^2, \tag{1}$$

a plane-wave incident field with the incident direction $d \in S^1$ and (real-valued) wave number $k > 0$, and consider the direct obstacle scattering problem to find the total field $u = u^i + u^s$ satisfying the Helmholtz equation

$$\Delta u + k^2 u = 0 \qquad \text{in } \mathbb{R}^2 \setminus \overline{D}, \tag{2}$$

the Sommerfeld radiation condition

$$\lim_{r\to\infty} \sqrt{r}\left(\frac{\partial u^s}{\partial r} - \mathrm{i}ku^s\right) = 0 \qquad \text{for} \quad r = |x|, \tag{3}$$

uniformly with respect to $\hat{x} = x/|x| \in S^1$ for the scattered field u^s, and one of the following three boundary conditions (the same for all scatterers):

$$\text{Dirichlet boundary condition (DBC)} \quad u = 0 \quad \text{on } \partial D_l, \tag{4a}$$

$$\text{Impedance boundary condition (IBC)} \quad \frac{\partial u}{\partial \nu} + \mathrm{i}\lambda_l k u = 0 \quad \text{on } \partial D_l, \tag{4b}$$

$$\text{Neumann boundary condition (NBC)} \quad \frac{\partial u}{\partial \nu} = 0 \quad \text{on } \partial D_l, \tag{4c}$$

$1 \leqslant l \leqslant L$. In acoustic scattering the pressure of the total wave vanishes on the boundary of an obstacle carrying a Dirichlet boundary condition and accordingly these are called sound soft. Scatterers with a Neumann boundary condition are called sound hard because the normal velocity of the total wave vanishes on the boundary of the object, and in the case of the impedance boundary condition, where the normal velocity on the boundary is proportional to the excess pressure on the boundary, $\lambda_l \in C(\partial D_l)$, $\lambda_l > 0$, denotes the so-called surface impedance (see Colton and Kress [13, p 13–5]). In the following we will use this terminology and note the results that apply to two-dimensional electromagnetic scattering accordingly.

It is well known that the system (2)–(3), together with any of the boundary conditions in (4), has a unique solution (see, e.g., Colton and Kress [12, theorems 3.21, 3.25, and 3.38]). Furthermore, the radiation condition (3) implies the asymptotic behavior

$$u^s(x; d, k) = \frac{\mathrm{e}^{\mathrm{i}k|x|}}{\sqrt{|x|}} u^\infty(\hat{x}; d, k) + O(|x|^{-3/2}) \tag{5}$$

for $|x| \to \infty$, where $\hat{x} := x/|x|$ and the so-called far-field pattern is given by

$$u^\infty(\hat{x}; d, k) = \frac{\mathrm{e}^{\mathrm{i}\pi/4}}{\sqrt{8\pi k}} \int_{\partial D} \left(u^s(y; d, k) \frac{\partial\, \mathrm{e}^{-\mathrm{i}k\hat{x}\cdot y}}{\partial \nu(y)} - \frac{\partial u^s(y; d, k)}{\partial \nu(y)} \mathrm{e}^{-\mathrm{i}k\hat{x}\cdot y} \right) \mathrm{d}s(y).$$

(cf [13, p 66–7]).

We are interested in the inverse scattering problem[1] to recover the support of the scatterers $D_1, \ldots, D_l$ given far-field patterns $u^\infty(\,\cdot\,; d_m, k_n)$ corresponding to incident fields with one or a few different incident directions $d_1, \ldots, d_M \in S^1$ and several wave numbers $k_1, \ldots, k_N > 0$. These far fields are assumed to be known on the whole unit circle, i.e. we are concerned with full aperture scattering data. Throughout, unless otherwise stated, we assume that the diameter of the scatterers is small compared to the wavelengths of the incident fields and that

[1] For a detailed introduction to inverse scattering problems we refer to [13].

the scatterers are well-separated, i.e. they do not intersect and are a fixed distance away from each other. To exploit this assumption we consider in the next section the asymptotic behavior of the far-field pattern as the diameter of the scatterers tends to zero relative to the wavelength. In contrast to fixed frequency expansions as, e.g., considered in [5, 38], we explicitly track down the dependence of these formulas on the wave number k. This is important when the expansions are applied to study the multi-frequency reconstruction method in section 4.

3. Small volume expansions

To study the asymptotic behavior of the far-field pattern $u^\infty(\cdot\,;d,k)$ as the scatterers $D_1,\ldots,D_L$ become small with respect to the wavelength, we introduce a scalable version of these scatterers, $D_{\rho,l} := z_l + \rho B_l$, $1 \leqslant l \leqslant L$, where $z_l \in \mathbb{R}^2$ describes the position of the scatterers, $0 < \rho < \rho_0$ their size, and $B_l \subset \mathbb{R}^2$ with $0 \in B_l$ their relative shape. Here ρ_0 is such that the scatterers $D_{\rho,1},\ldots,D_{\rho,L}$ are well-separated for $0 < \rho < \rho_0$. If there is only a single scatterer, then $\rho_0 = \infty$. Accordingly, we write in the following $u^s_\rho(\cdot\,;d,k)$ and $u^\infty_\rho(\cdot\,;d,k)$ for the scattered field and the far-field pattern corresponding to $D_\rho := \bigcup_{l=1}^L D_{\rho,l}$, respectively. Using ideas from [3, 16], we derive the leading-order term in the asymptotic expansion of $u^\infty_\rho(\cdot\,;d,k)$ with respect to $k\rho$ as $k\rho \to 0$ with $k > k_0$, where k_0 is a lower bound for the wave number satisfying $k_0 > 0$ if there are multiple scatterers and $k_0 = 0$ if there is only a single scatterer.

The main results of this section are summarized in the following theorem.

Theorem 3.1. *Let $u^\infty_\rho(\cdot\,;d,k) \in L^2(S^1)$ denote the far-field pattern of the scattered field $u^s_\rho(\cdot\,;d,k)$ corresponding to the solution $u_\rho(\cdot\,;d,k) = u^i(\cdot\,;d,k) + u^s_\rho(\cdot\,;d,k)$ of (2) and (3) with the incident field $u^i(\cdot\,;d,k)$ from (1), the scatterers $D_{\rho,l} = z_l + \rho B_l$, $1 \leqslant l \leqslant L$, and one of the boundary conditions described in (4). Then, as $k\rho \to 0$ with $k > k_0$ and $\rho < \rho_0$; the far-field pattern corresponding to the Dirichlet boundary condition (4a) satisfies*

$$\sqrt{k}u^\infty_\rho(\hat{x};d,k) = \frac{1}{\log(k\rho)}2\pi\frac{e^{i\pi/4}}{\sqrt{8\pi}}\sum_{l=1}^{L} e^{ik(d-\hat{x})\cdot z_l} + \mathcal{O}\left(\frac{1}{(\log(k\rho))^2}\right), \tag{6a}$$

the far-field pattern corresponding to the impedance boundary condition (4b) satisfies

$$\sqrt{k}u^\infty_\rho(\hat{x};d,k) = ik\rho\frac{e^{i\pi/4}}{\sqrt{8\pi}}\sum_{l=1}^{L} \overline{\lambda}_l|\partial B_l|\, e^{ik(d-\hat{x})\cdot z_l} + \mathcal{O}(\lambda k^2\rho^2\log(k\rho)), \tag{6b}$$

and the far-field pattern corresponding to the Neumann boundary condition (4c) satisfies

$$\sqrt{k}u^\infty_\rho(\hat{x};d,k) = -k^2\rho^2\frac{e^{i\pi/4}}{\sqrt{8\pi}}\sum_{l=1}^{L}\left(|B_l| + \hat{x}\cdot\mathbb{M}^0_{B_l}d\right)e^{ik(d-\hat{x})\cdot z_l} + \mathcal{O}(k^3\rho^3\log(k\rho)), \tag{6c}$$

uniformly with respect to $\hat{x} \in S^1$. In (6b) we use the notation $\overline{\lambda}_l := \int_{\partial D_{\rho,l}} \lambda_l\, ds/|\partial D_{\rho,l}|$ and in (6c) $\mathbb{M}^0_{B_l}$ denotes the polarization tensor corresponding to the sound-hard scatterer $D_{\rho,l}$ as introduced in the following (20).

Remark 3.2 (Penetrable scatterers)**.** Considering electromagnetic scattering and denoting by ε_0 and μ_0 the electric permittivity and the magnetic permeability of free space, respectively, $\omega := k/\sqrt{\varepsilon_0\mu_0}$ is called the angular frequency of the incident field. If the scatterers are not impenetrable as above but filled with a penetrable medium specified by an electric permittivity

ε_1, an electric conductivity σ_1, and a magnetic permeability μ_1 (all constant, say), then scattering of the incoming wave $u^i(\cdot\,; d, k)$ by this object is described by the equation

$$\nabla \cdot \left(\frac{1}{\mu_\rho}\nabla u_\rho\right) + \omega^2 \varepsilon_\rho u_\rho = 0 \qquad \text{in} \quad \mathbb{R}^2$$

together with the Sommerfeld radiation condition (3) for $u^s_\rho = u_\rho - u^i$. Here,

$$\mu_\delta(x) := \begin{cases} \mu_1, & x \in D_\delta, \\ \mu_0, & x \in \Omega \setminus \overline{D_\delta}, \end{cases} \qquad \varepsilon_\delta(x) := \begin{cases} \tilde{\varepsilon}_1, & x \in D_\delta, \\ \varepsilon_0, & x \in \Omega \setminus \overline{D_\delta} \end{cases}$$

denote the piecewise constant material parameters with $\tilde{\varepsilon}_1 := \varepsilon_1 + \mathrm{i}\frac{\sigma_1}{\omega}$. The asymptotic behavior of the corresponding far-field pattern u^∞_ρ has been studied for different frequency ranges in [19]. It has been shown that

$$\sqrt{k}u^\infty_\rho(\hat{x}; d, k) = -k^2\rho^2 \frac{\mathrm{e}^{\mathrm{i}\pi/4}}{\sqrt{8\pi}} \sum_{l=1}^{L} \left(\left(1 - \frac{\tilde{\varepsilon}_1}{\varepsilon_0}\right)|B_l| + \frac{\mu_1}{\mu_0}\hat{x} \cdot \mathbb{M}^{\mu_0/\mu_1}_{B_l} d\right) \mathrm{e}^{\mathrm{i}k(d-\hat{x})\cdot z_l} + o(k^2\rho^2) \tag{7}$$

as $k\rho \to 0$. Here the polarization tensor $\mathbb{M}^{\mu_0/\mu_1}_{B_l} \in \mathbb{R}^{2\times 2}$, $1 \leqslant l \leqslant L$, corresponding to $D_{\rho,l}$ and the permeability contrast μ_0/μ_1 is defined by

$$\mathbb{M}^{\mu_0/\mu_1}_{B_l} := \int_{\partial B_l} \eta \left(\left(\frac{\mu_1 + \mu_0}{2(\mu_1 - \mu_0)} I + {K^0_{B_l}}^\top\right)^{-1} \nu\right)^\top (\eta)\, \mathrm{d}s(\eta),$$

where ${K^0_{B_l}}^\top$ is the transpose of the double layer operator introduced in section 3.2 in the following (see, e.g., [6] for further results on this polarization tensor).

Although we consider in the following impenetrable scatterers only, we note that because of the similar structure of the asymptotic expansions (7) and (6*c*), the results obtained for obstacles carrying a Neumann boundary condition can be applied to penetrable scatterers accordingly.

The next two subsections are devoted to the proof of theorem 3.1. To simplify the presentation, we restrict ourselves to the case of a single scatterer $D_\rho = z + \rho B$, i.e. $L = 1$. However, the proofs can be generalized to multiple scatterers straightforwardly as, e.g., outlined for an electrostatic problem in section 6 of [3]. Here the assumptions $\rho < \rho_0 < \infty$ such that the scatterers stay well-separated and $k > k_0 > 0$ ensure that multiple scattering effects can be estimated by the $\mathcal{O}$-terms in (6) as $k\rho \to 0$.

3.1. Asymptotic behavior of the fundamental solution

Before we consider the scattered field, we study the asymptotic behavior of the fundamental solution to the Helmholtz equation

$$\Phi_k(x, y) := \frac{\mathrm{i}}{4} H^{(1)}_0(k|x - y|), \qquad x \neq y,$$

where $H^{(1)}_0$ denotes the Hankel function of the first kind of order 0, for small values of $k|x - y|$ as well as for large values of $|x|$.

Recalling that $H^{(1)}_n = J_n + \mathrm{i}\, Y_n$, where J_n and Y_n are the Bessel function and Neumann function of order n, respectively, we find from the series expansions of these functions (see [13, (3.51) and (3.52)]) that for $k|x - y| \to 0$,

$$\Phi_k(x, y) = \Phi_0(x, y) + \left(\frac{\mathrm{i}}{4} - \frac{1}{2\pi}\log\frac{k}{2} - \frac{C_E}{2\pi}\right) + \mathcal{O}(k^2|x - y|^2 \log(k|x - y|)), \qquad x \neq y, \tag{8}$$

and

$$\frac{1}{k}\nabla_y \Phi_k(x,y) = \frac{1}{k}\nabla_y \Phi_0(x,y) - \frac{1}{4\pi}k(x-y)\log(k|x-y|) + \left(\frac{\mathrm{i}}{8} + \frac{\log 2}{4\pi} - \frac{C_E}{4\pi} + \frac{1}{8\pi}\right)k(x-y) + \mathcal{O}(k^3|x-y|^3\log(k|x-y|)), \qquad x \neq y, \tag{9}$$

where $\Phi_0(x,y) := -(1/2\pi)\log|x-y|$ denotes the fundamental solution for the Laplace equation and $C_E = 0.577\,215\,66\cdots$ is Euler's constant.

On the other hand, it follows from the asymptotic behavior of the Hankel functions

$$H_n^{(1)}(t) = \sqrt{\frac{2}{\pi t}}\,\mathrm{e}^{\mathrm{i}(t-\frac{n\pi}{2}-\frac{\pi}{4})} + O(t^{-3/2}), \qquad t \to \infty, \tag{10}$$

(cf [13, (3.59)]) that the far-field pattern of the fundamental solution is given by

$$\Phi_k^\infty(\hat{x},y) = \frac{\mathrm{e}^{\mathrm{i}\pi/4}}{\sqrt{8\pi k}}\,\mathrm{e}^{-\mathrm{i}k\hat{x}\cdot y}. \tag{11}$$

To obtain a similar result for its gradient we observe that

$$\nabla_y \Phi_k(x,y) = \frac{\mathrm{i}}{4}H_1^{(1)}(k|x-y|)k\frac{x-y}{|x-y|}, \qquad x \neq y,$$

and expand near infinity to see that for any $p \in \mathbb{R}^2$,

$$\frac{(x-y)\cdot p}{|x-y|} = (|x|\hat{x}\cdot p - y\cdot p)\frac{1}{|x|}(1+\mathcal{O}(|x|^{-1})) = \hat{x}\cdot p + \mathcal{O}(|x|^{-1})$$

as $|x| \to \infty$. Therefore, using (10) once more,

$$(\nabla_y \Phi_k \cdot p)^\infty(\hat{x},y) = k\hat{x}\cdot p\frac{\mathrm{e}^{-\mathrm{i}\pi/4}}{\sqrt{8\pi k}}\,\mathrm{e}^{-\mathrm{i}k\hat{x}\cdot y}. \tag{12}$$

3.2. Asymptotic expansion of the scattered field

We start by introducing some convenient notation to deal with changes of coordinates. For $x, y \in \partial D_\rho$ we define $\xi := (x-z)/\rho$ and $\eta := (y-z)/\rho$, which are both in ∂B. Accordingly, we may rescale any $\phi \in C(\partial D_\rho)$ and any $\psi \in C(\partial B)$ by means of

$$(\phi)^\wedge(\xi) := \hat{\phi}(\xi) := \phi(z+\rho\xi) \qquad \text{and} \qquad (\psi)^\vee(x) := \check{\psi}(x) := \psi\left(\frac{x-z}{\rho}\right)$$

to obtain $(\phi)^\wedge, \hat{\phi} \in C(\partial B)$ and $(\psi)^\vee, \check{\psi} \in C(\partial D_\rho)$, respectively.

Recalling the definition the single- and double-layer operator $S_{D_\rho} : C(\partial D_\rho) \to C(\partial D_\rho)$ and $K_{D_\rho} : C(\partial D_\rho) \to C(\partial D_\rho)$ given by

$$(S_{D_\rho}\phi)(x) := \int_{\partial D_\rho} \phi(y)\Phi_k(x,y)\,\mathrm{d}s(y), \qquad x \in \partial D_\rho,$$

$$(K_{D_\rho}\phi)(x) := \int_{\partial D_\rho} \phi(y)\frac{\partial \Phi_k(x,y)}{\partial \nu(y)}\,\mathrm{d}s(y), \qquad x \in \partial D_\rho,$$

respectively, we denote by $K_{D_\rho}^\top$ the dual of K_{D_ρ} with respect to the dual system $\langle C(\partial D_\rho), C(\partial D_\rho)\rangle$ (see [12, theorem 1.23]). Similarly, let $S_{D_\rho}^0$, $K_{D_\rho}^0$ and ${K_{D_\rho}^0}^\top$ be the corresponding operators with Φ_k replaced by Φ_0, and define $M_{D_\rho}^0 : C(\partial D_\rho) \to C(\partial D_\rho)$,

$$\left(M_{D_\rho}^0\phi\right)(x) := \frac{1}{2\pi}\int_{\partial D_\rho} \psi(y)\,\mathrm{d}s(y).$$

In the following we first show (6*a*) corresponding to the Dirichlet boundary condition and then continue with the proof of (6*b*) and (6*c*).

It is well known that the scattered field u_ρ^s corresponding to the Dirichlet boundary condition (4*a*) can be written as a combined double- and single-layer potential

$$u_\rho^s(x;d,k) = \int_{\partial D_\rho} \left(\frac{\partial \Phi_k(x,y)}{\partial \nu(y)} - \mathrm{i}\gamma \Phi_k(x,y) \right) \phi(y)\, \mathrm{d}s(y), \qquad x \in \mathbb{R}^2 \setminus \overline{D_\rho}, \tag{13}$$

with a real coupling parameter $\gamma \neq 0$, provided the density $\phi \in C(\partial D_\rho)$ satisfies the integral equation

$$\tfrac{1}{2}\phi + K_{D_\rho}\phi - \mathrm{i}\gamma S_{D_\rho}\phi = -u^i(\cdot;d,k)$$

on ∂D_ρ. From [13, p 48] we find that the integral operator

$$\tfrac{1}{2} I + K_{D_\rho} - \mathrm{i}\gamma S_{D_\rho} : C(\partial D_\rho) \to C(\partial D_\rho),$$

where I denotes the identity operator, is bijective and its inverse is bounded. The following lemma describes the scaling properties of this operator under changes of variables as introduced above.

Lemma 3.3. *Let $\phi \in C(\partial D_\rho)$ and choose $\gamma = \frac{1}{\rho \log(k\rho)}$. Then,*

$$\left(\frac{1}{2} I + K_{D_\rho} - \mathrm{i}\gamma S_{D_\rho} \right) \phi = \left(\left(\frac{1}{2} I + K_B^0 + \mathrm{i} M_B^0 \right) \hat{\phi} \right)^\vee + \mathcal{O}\left(\frac{1}{\log(k\rho)} \right), \tag{14}$$

uniformly on compact subsets of $C(\partial D_\rho)$ as $k\rho \to 0$.

Proof. For $\phi \in C(\partial D_\rho)$ we find by change of variables that

$$\begin{aligned} \left(K_{D_\rho}^0 \phi\right)(x) &= \frac{1}{2\pi} \int_{\partial D_\rho} \frac{(x-y)\cdot \nu(y)}{|x-y|^2} \phi(y)\, \mathrm{d}s(y) \\ &= \frac{1}{2\pi} \int_{\partial B} \frac{1}{\rho} \frac{(\xi-\eta)\cdot \nu(\eta)}{|\xi-\eta|^2} \hat{\phi}(\eta) \rho\, \mathrm{d}s(\eta) = \left(K_B^0 \hat{\phi}\right)(\xi). \end{aligned} \tag{15}$$

Since by (9)

$$\begin{aligned} \frac{1}{k} \nabla_y (\Phi_k - \Phi_0)(x,y) &= -\frac{1}{4\pi} k(x-y) \log(k|x-y|) + \mathcal{O}(k|x-y|) \\ &= -\frac{1}{4\pi} k\rho(\xi-\eta)(\log(k\rho) + \log|\xi-\eta|) + \mathcal{O}(k\rho) \end{aligned}$$

as $k\rho \to 0$, we obtain for any $x \in \partial D_\rho$ that

$$\begin{aligned} ((K_{D_\rho} - K_{D_\rho}^0)\phi)(x) &= \int_{\partial D_\rho} \phi(y) \nu(y) \cdot \nabla_y (\Phi_k - \Phi_0)(x,y)\, \mathrm{d}s(y) \\ &= \int_{\partial B} \hat{\phi}(\eta) \nu(\eta) \cdot \left(-\frac{k^2}{4\pi} \rho(\xi-\eta)(\log(k\rho) \right. \\ &\quad \left. + \log|\xi-\eta|) + \mathcal{O}(k^2\rho) \right) \rho\, \mathrm{d}s(\eta) \\ &= \mathcal{O}(k^2\rho^2 \log(k\rho)) \end{aligned} \tag{16}$$

uniformly with respect to $x \in \partial D_\rho$ and uniformly on compact subsets of $C(\partial D_\rho)$.

Similarly,

$$\begin{aligned}\big(S^0_{D_\rho}\phi\big)(x) &= -\int_{\partial D_\rho} \frac{1}{2\pi}\log|x-y|\phi(y)\,\mathrm{d}s(y)\\ &= -\int_{\partial B}\frac{1}{2\pi}(\log\rho+\log|\xi-\eta|)\hat\phi(\eta)\rho\,\mathrm{d}s(\eta)\\ &= -\rho\log\rho\big(M^0_B\hat\phi\big)(\xi)+\rho\big(S^0_B\hat\phi\big)(\xi).\end{aligned}$$

From (8) we find that

$$(\Phi_k-\Phi_0)(x,y)=\frac{\mathrm{i}}{4}-\frac{1}{2\pi}\log\frac{k}{2}-\frac{C_E}{2\pi}+\mathcal{O}(k^2\rho^2\log(k\rho))$$

as $k\rho\to 0$, and thus

$$\begin{aligned}\big(\big(S_{D_\rho}-S^0_{D_\rho}\big)\phi\big)(x) &= \int_B\left(\frac{\mathrm{i}}{4}-\frac{1}{2\pi}\log\frac{k}{2}-\frac{C_E}{2\pi}+\mathcal{O}(k^2\rho^2\log(k\rho))\right)\hat\phi(\eta)\rho\,\mathrm{d}s(\eta)\\ &= \rho\left(\frac{\mathrm{i}\pi}{2}-\log k+\log 2-C_E\right)\big(M^0_B\hat\phi\big)(\xi)+\mathcal{O}(k^2\rho^3\log(k\rho)).\end{aligned}$$

Therefore,

$$\begin{aligned}\frac{1}{\rho\log(k\rho)}(S_{D_\rho}\phi)(x) &= -\big(M^0_B\hat\phi\big)(\xi)+\frac{1}{\log(k\rho)}\big(S^0_B\hat\phi\big)(\xi)\\ &\quad+\frac{1}{\log(k\rho)}\left(\frac{\mathrm{i}\pi}{2}+\log 2-C_E\right)\big(M^0_B\hat\phi\big)(\xi)+\mathcal{O}(k^2\rho^2).\end{aligned}\tag{17}$$

Combining (15), (16), and (17) yields (14). □

It can be seen as in [26, theorem 6.24] that the operator

$$\tfrac{1}{2}I+K^0_B+\mathrm{i}M^0_B : C(\partial B)\to C(\partial B)$$

is bijective and its inverse is bounded. Furthermore, recalling that $K^0_B 1=-1/2$ (cf [26, p 79]) a short computation shows that its transpose

$$\tfrac{1}{2}I+{K^0_B}^{\top}+\mathrm{i}M^0_B : C(\partial B)\to C(\partial B)$$

maps

$$C_\diamond(\partial B):=\left\{\psi\in C(\partial B)\,\middle|\,\int_{\partial B}\psi\,\mathrm{d}s=0\right\}$$

onto itself. Lemma 3.3 yields that for $\gamma=1/(\rho\log(k\rho))$ and for any $\psi\in C(\partial D_\rho)$,

$$\left(\frac{1}{2}I+K_{D_\rho}-\mathrm{i}\gamma S_{D_\rho}\right)^{-1}\psi=\left(\left(\frac{1}{2}I+K^0_B+\mathrm{i}\,M^0_B\right)^{-1}\hat\psi\right)^{\vee}+\mathcal{O}\left(\frac{1}{\log(k\rho)}\right),\tag{18}$$

uniformly on compact subsets of $C(\partial D_\rho)$ (see [26, theorem 10.1]).

Now let $R>0$ large enough such that $D_\rho\subset B_R(0)$. Choosing $\gamma=1/(\rho\log(k\rho))$ in (13) and writing $g:=-u^i(\,\cdot\,;d,k)$,

$$u^s_\rho\big|_{\partial B_R(0)}=\int_{\partial D_\rho}\left(\frac{\partial\Phi_k(\cdot,y)}{\partial\nu(y)}-\mathrm{i}\gamma\Phi_k(\cdot,y)\right)\left(\left(\frac{1}{2}I+K_{D_\rho}-\mathrm{i}\gamma S_{D_\rho}\right)^{-1}g\right)(y)\,\mathrm{d}s(y).$$

Letting $R\to\infty$, recalling (5), we use a change of coordinates, Taylor expansions, and (18) to estimate

$$u_\rho^\infty(\hat{x};d,k) = \int_{\partial D_\rho} \left(\frac{\partial \Phi_k^\infty(\hat{x},y)}{\partial \nu(y)} - \mathrm{i}\gamma \Phi_k^\infty(\hat{x},y) \right) \left(\left(\frac{1}{2} I + K_{D_\rho} - \mathrm{i}\gamma S_{D_\rho} \right)^{-1} g \right)(y)\, \mathrm{d}s(y)$$

$$= \int_{\partial B} \nu(\eta) \cdot (\nabla_y \Phi_k^\infty(\hat{x},z) + \mathcal{O}(k^{3/2}\rho))$$

$$\times \left(\left(\frac{1}{2} I + K_B^0 + \mathrm{i}\, M_B^0 \right)^{-1} \hat{g} + \mathcal{O}\left(\frac{1}{\log(k\rho)} \right) \right)(\eta)\rho\, \mathrm{d}s(\eta)$$

$$- \frac{\mathrm{i}}{\rho \log(k\rho)} \int_{\partial B} \left(\Phi_k^\infty(\hat{x},z) + \mathcal{O}(k^{1/2}\rho) \right)$$

$$\times \left(\left(\frac{1}{2} I + K_B^0 + \mathrm{i} M_B^0 \right)^{-1} \hat{g} + \mathcal{O}\left(\frac{1}{\log(k\rho)} \right) \right)(\eta)\rho\, \mathrm{d}s(\eta).$$

Expanding the incident field $u^i(\,\cdot\,;d,k)$ around z yields

$$u_\rho^\infty(\hat{x};d,k) = \frac{\mathrm{i}}{\log(k\rho)} \Phi_k^\infty(\hat{x},z) \int_{\partial B} \left(\left(\frac{1}{2} I + K_B^{0\,\top} + \mathrm{i} M_B^0 \right)^{-1} 1 \right)(\eta)(u^i(z;d,k)$$

$$+ \mathcal{O}(k\rho))\, \mathrm{d}s(\eta) + \mathcal{O}\left(\frac{1}{\sqrt{k}} \frac{1}{(\log(k\rho))^2} \right).$$

Now observing that

$$\int_{\partial B} \left(\left(\frac{1}{2} I + K_B^0 + \mathrm{i} M_B^0 \right)^{-1} 1 \right)(\eta)\, \mathrm{d}s(\eta) = \frac{2\pi}{\mathrm{i}}$$

because $K_B^0 1 = -1/2$, we obtain that

$$\sqrt{k} u_\rho^\infty(\hat{x};d,k) = \frac{1}{\log(k\rho)} 2\pi \sqrt{k} \Phi_k^\infty(\hat{x},z) u^i(z;d,k) + \mathcal{O}\left(\frac{1}{(\log(k\rho))^2} \right),$$

uniformly with respect to $\hat{x} \in S^1$. This is (6*a*).

Next we show simultaneously the asymptotic expansions (6*b*) and (6*c*). To this end we introduce

$$\alpha := \begin{cases} \lambda & \text{if} \quad \partial D_\rho \text{ carries the impedance boundary condition } (4b), \\ 0 & \text{if} \quad \partial D_\rho \text{ carries the Neumann boundary condition } (4c), \end{cases}$$

and write the scattered field as a single layer potential

$$u_\rho^s(x;d,k) = \int_{\partial D_\rho} \Phi_k(x,y) \psi(y)\, \mathrm{d}s(y),$$

where the density $\psi \in C(\partial D_\rho)$ satisfies

$$-\frac{1}{2}\psi + K_{D_\rho}^\top \psi + \mathrm{i}\alpha k S_{D_\rho} \psi = -\frac{\partial u^i}{\partial \nu}(\cdot;d,k) - \mathrm{i}\alpha k u^i(\cdot;d,k) \qquad \text{on} \quad \partial D_\rho.$$

The integral operator $-\frac{1}{2} I + K_{D_\rho}^\top + \mathrm{i}\alpha k S_{D_\rho} : C(\partial D_\rho) \to C(\partial D_\rho)$ is compact and one-to-one, provided that k is not a Dirichlet eigenvalue for D_ρ (cf, e.g., [12, p 98]). Denoting by $(k_j^B)_{j\in\mathbb{N}}$ the discrete set of real Dirichlet eigenvalues corresponding to the reference domain B in the increasing order, which accumulates only at infinity (cf [12, p 77]), it follows from the variational formulation of the eigenvalue problem that the Dirichlet eigenvalues corresponding to D_ρ are given by $(\rho^{-1} k_j^B)_{j\in\mathbb{N}}$. Since we are interested in the asymptotic behavior of u_ρ^s as $k\rho \to 0$ we may assume henceforth without loss of generality that $k\rho < k_1^B$, such that k is not a Dirichlet eigenvalue for D_ρ.

Similar to lemma 3.3 we consider in the following lemma the scaling properties of the operator $-\frac{1}{2} I + K_{D_\rho}^\top + \mathrm{i}\alpha k S_{D_\rho}$.

Lemma 3.4. *Let $\psi \in C(\partial D_\rho)$ and α as introduced above. Then,*

$$\begin{aligned}\left(-\frac{1}{2}I + K_{D_\rho}^\top + \mathrm{i}\,\alpha k S_{D_\rho}\right)\psi &= \left(\left(-\frac{1}{2}I + K_B^{0\top} + \mathrm{i}\hat{\alpha}k\rho\left(S_B^0 + \left(\frac{\mathrm{i}\pi}{2} - \log\frac{k\rho}{2} - C_E\right)M_B^0\right)\right)\hat{\psi}\right)^\vee + \mathcal{O}(k^2\rho^2\log(k\rho)) \\ &= \left(\left(-\frac{1}{2}I + K_B^{0\top}\right)\hat{\psi}\right)^\vee + \mathcal{O}(\alpha k\rho\log(k\rho)) + \mathcal{O}(k^2\rho^2\log(k\rho)),\end{aligned}$$

uniformly on compact subsets of $C(\partial D_\rho)$.

Proof. As in (15) and (16) we find that

$$K_{D_\rho}^\top\psi = \left(K_B^{0\top}\hat{\psi}\right)^\vee + \mathcal{O}(k^2\rho^2\log(k\rho)).$$

So, recalling (17) yields the desired result. □

The operator

$$-\tfrac{1}{2}I + K_B^{0\top} : C(\partial B) \to C(\partial B)$$

is bijective, maps $C_\diamond(\partial B)$ onto itself, and its inverse is bounded (see [26, theorem 6.20]). Therefore, still assuming that $k\rho$ is small enough, for any $\psi \in C(\partial D_\rho)$:

$$\begin{aligned}\left(-\tfrac{1}{2}I + K_{D_\rho}^\top + \mathrm{i}\alpha k S_{D_\rho}\right)^{-1}\psi &= \left(\left(-\tfrac{1}{2}I + K_B^{0\top}\right)^{-1}\hat{\psi}\right)^\vee \\ &\quad + \mathcal{O}(\alpha k\rho\log(k\rho)) + \mathcal{O}(k^2\rho^2\log(k\rho)),\end{aligned} \tag{19}$$

uniformly on compact subsets of $C(\partial D_\rho)$.

Let again $R > 0$ large enough such that $D_\rho \subset B_R(0)$ and write $f := -\frac{\partial u^i}{\partial \nu}(\,\cdot\,; d, k) - \mathrm{i}\alpha k u^i(\,\cdot\,; d, k))$. Then,

$$u_\rho^s|_{\partial B_R(0)} = \int_{\partial D_\rho} \Phi_k(\cdot, y)\left(\left(-\frac{1}{2}I + K_{D_\rho}^\top + \mathrm{i}\alpha k S_{D_\rho}\right)^{-1} f\right)(y)\,\mathrm{d}s(y).$$

Letting $R \to \infty$, recalling (5), we use a change of coordinates, Taylor expansions, and (19) to estimate

$$\begin{aligned}u_\rho^\infty(\hat{x}; d, k) &= \int_{\partial D_\rho} \Phi_k^\infty(\hat{x}, y)\left(\left(-\frac{1}{2}I + K_{D_\rho}^\top + \mathrm{i}\alpha k S_{D_\rho}\right)^{-1} f\right)(y)\,\mathrm{d}s(y) \\ &= \int_{\partial B} \left(\Phi_k^\infty(\hat{x}, z) + \rho\eta\cdot\nabla_y\Phi_k^\infty(\hat{x}, z) + \mathcal{O}(k^{3/2}\rho^2)\right)\left(\left(-\frac{1}{2}I + K_B^{0\top}\right)^{-1}\hat{f}\right. \\ &\quad \left. + \mathcal{O}(\alpha k^2\rho\log(k\rho)) + \mathcal{O}(k^3\rho^2\log(k\rho))\right)(\eta)\rho\,\mathrm{d}s(\eta).\end{aligned}$$

Expanding the incident field $u^i(\,\cdot\,; d, k)$ and its normal derivative $(\partial u^i/\partial\nu)(\,\cdot\,; d, k)$ around z yields

$$\begin{aligned}u_\rho^\infty(\hat{x}; d, k) &= \rho\Phi_k^\infty(\hat{x}, z)\int_{\partial B}\left(\left(-\frac{1}{2}I + K_B^{0\top}\right)^{-1}(-\nu(\eta)\cdot\nabla u^i(z; d, k) - \rho\nu(\eta)\right. \\ &\quad \left.\cdot\nabla^\top\nabla u^i(z; d, k)\eta + \mathcal{O}(k^3\rho^2) - \mathrm{i}\hat{\alpha}k(u^i(z; d, k) + \mathcal{O}(k\rho)))\right)(\eta)\,\mathrm{d}s(\eta) \\ &\quad + \rho^2\nabla_y\Phi_k^\infty(\hat{x}, z)\cdot\int_{\partial B}\eta\left(\left(-\frac{1}{2}I + K_B^{0\top}\right)^{-1}(-\nu(\eta)\cdot\nabla u^i(z; d, k)\right. \\ &\quad \left. + \mathcal{O}(k^2\rho) + \mathcal{O}(\alpha k))\right)(\eta)\,\mathrm{d}s(\eta) + \mathcal{O}(\alpha k^{3/2}\rho^2\log(k\rho)) + \mathcal{O}(k^{5/2}\rho^3\log(k\rho)).\end{aligned}$$

Since $K_B^0 1 = -1/2$,

$$\left(-\frac{1}{2}I + K_B^0\right)^{-1} 1 = -1,$$

and thus, recalling Gauss' theorem, we obtain

$$\begin{aligned} u_\rho^\infty(\hat{x}; d, k) = {} & \mathrm{i}k\rho\overline{\alpha}|\partial B|\Phi_k^\infty(\hat{x}, z)u^i(z; d, k) + \rho^2\Phi_k^\infty(\hat{x}, z)\int_B \mathrm{div}_\eta(\nabla^\top\nabla u^i(z; d, k)\eta)\,\mathrm{d}\eta \\ & - \rho^2\nabla_y\Phi_k^\infty(\hat{x}, z)\cdot\int_{\partial B}\eta\left(\left(-\frac{1}{2}I + {K_B^0}^\top\right)^{-1}\nu\right)^\top(\eta)\mathrm{d}s(\eta)\nabla u^i(z; d, k) \\ & + \mathcal{O}(\alpha k^{3/2}\rho^2\log(k\rho)) + \mathcal{O}(k^{5/2}\rho^3\log(k\rho)). \end{aligned}$$

Defining the polarization tensor $\mathbb{M}_B^0 \in \mathbb{R}^{2\times 2}$ corresponding to B by

$$\mathbb{M}_B^0 := -\int_{\partial B}\eta\left(\left(-\frac{1}{2}I + {K_B^0}^\top\right)^{-1}\nu\right)^\top(\eta)\,\mathrm{d}s(\eta) \tag{20}$$

(see, e.g., [6]) and observing that

$$\mathrm{div}_\eta(\nabla^\top\nabla u^i(z; d, k)\eta) = \Delta u^i(z; d, k) = -k^2 u^i(z; d, k)$$

we find that

$$\begin{aligned} \sqrt{k}u_\rho^\infty(\hat{x}; d, k) = {} & \mathrm{i}k\rho\overline{\alpha}|\partial B|\sqrt{k}\Phi_k^\infty(\hat{x}, z)u^i(z; d, k) \\ & + k^2\rho^2\big(-|B|\sqrt{k}\Phi_k^\infty(\hat{x}, z)u^i(z; d, k) + k^{-3/2}\nabla_y\Phi_k^\infty(\hat{x}, z)\cdot\mathbb{M}_B^0\nabla u^i(z; d, k)\big) \\ & + \mathcal{O}(\alpha k^2\rho^2\log(k\rho)) + \mathcal{O}(k^3\rho^3\log(k\rho)), \end{aligned}$$

uniformly with respect to $\hat{x} \in S^1$. This implies (6*b*) for $\alpha = \lambda$ and (6*c*) for $\alpha = 0$.

4. Multi-frequency orthogonality sampling

Now we assume that far-field patterns $u_\rho^\infty(\,\cdot\,; d_m, k_n)$ corresponding to plane-wave incident fields $u^i(\,\cdot\,; d_m, k_n)$ with M incident directions $d_1, \ldots, d_m \in S^1$ and N frequencies $0 < k_1 < \cdots < k_N$ are given. The orthogonality sampling method as discussed by Potthast in [33] consists in evaluating the functional

$$\Im(y) := \sum_{n=1}^{N}\sum_{m=1}^{M} w_{mn}^\Im\left|\int_{S_1}\mathrm{e}^{\mathrm{i}k\hat{x}\cdot y}u^\infty(\hat{x}; d_m, k_n)\,\mathrm{d}s(\hat{x})\right|, \qquad y \in \mathbb{R}^2, \tag{21}$$

where the $w_{mn}^\Im$, $1 \leqslant m \leqslant M$ and $1 \leqslant n \leqslant N$, are weight functions that have to be chosen appropriately. It has been exemplified by a series of numerical experiments in [33] that visualizations of $\Im$ give a relatively clear image of the support of the scatterers. In the following we analyze this method based on the assumption that the product $k\rho$ of the wave number and relative size of the scatterers is sufficiently small such that we can approximate the far-field patterns by the leading order terms in (6), neglecting higher order terms. Based on this analysis we suggest some modifications to the original algorithm.

Assuming that all scatterers have the same (known) material properties, i.e. that they are either all sound soft, sound hard, or carry an impedance boundary condition, we observe from (6) that the magnitude of the far-field pattern strongly depends on the wave number of the incident field. To balance the information contained in the far-field patterns corresponding to different wave numbers, our first modification of the original algorithm is to rescale the far-field patterns appropriately. Similar to (21) we define for each incident direction d_m, each wave number k_n, and each $y \in \mathbb{R}^2$:

$$\text{DBC}: \quad \mathcal{I}(y;d_m,k_n) := \frac{1}{2\pi}\int_{S^1} \mathrm{e}^{\mathrm{i}k_n(\hat{x}-d_m)\cdot y}(-\mathrm{e}^{-\mathrm{i}\pi/4}\sqrt{8\pi k})u_\rho^\infty(\hat{x};d_m,k_n)\,\mathrm{d}s(\hat{x}), \tag{22a}$$

$$\text{IBC}: \quad \mathcal{I}(y;d_m,k_n) := \frac{1}{2\pi}\int_{S^1} \mathrm{e}^{\mathrm{i}k_n(\hat{x}-d_m)\cdot y}(-\mathrm{i}\,\mathrm{e}^{-\mathrm{i}\pi/4}k^{-1}\sqrt{8\pi k})u_\rho^\infty(\hat{x};d_m,k_n)\,\mathrm{d}s(\hat{x}), \tag{22b}$$

$$\text{NBC}: \quad \mathcal{I}(y;d_m,k_n) := \frac{1}{2\pi}\int_{S^1} \mathrm{e}^{\mathrm{i}k_n(\hat{x}-d_m)\cdot y}(-\mathrm{e}^{-\mathrm{i}\pi/4}k^{-2}\sqrt{8\pi k}))u_\rho^\infty(\hat{x};d_m,k_n)\,\mathrm{d}s(\hat{x}). \tag{22c}$$

In contrast to (21) we added an additional phase shift $\mathrm{e}^{-\mathrm{i}k_n d_m\cdot y}$ in (22). As we will see in the following, this guarantees that the values of $\mathcal{I}(\,\cdot\,;d_m,k_n)$ for $1\leqslant m\leqslant M$ and $1\leqslant n\leqslant N$ are coherent at the center of each scatterer $z_1,\ldots,z_m$. Thus, we can avoid taking absolute values as in (21) when combining the multi-frequency information in (27) below, which turns out to be important in our analysis.

Substituting the leading order terms of $u_\rho^\infty(\,\cdot\,;d_m,k_n)$ from (6) into (22), neglecting higher order terms, we obtain

$$\text{DBC}: \quad \mathcal{I}(y;d_m,k_n) \approx \frac{1}{2\pi}\,\mathrm{e}^{\mathrm{i}k_n(z_l-y)\cdot d_m}\int_{S^1}\mathrm{e}^{\mathrm{i}k_n(y-z_l)\cdot\hat{x}}\frac{1}{\log\rho}\,\mathrm{d}s(\hat{x}), \tag{23a}$$

$$\text{IBC}: \quad \mathcal{I}(y;d_m,k_n) \approx \frac{1}{2\pi}\,\mathrm{e}^{\mathrm{i}k_n(z_l-y)\cdot d_m}\int_{S^1}\mathrm{e}^{\mathrm{i}k_n(y-z_l)\cdot\hat{x}}\rho\overline{\lambda}_l|\partial B_l|\,\mathrm{d}s(\hat{x}), \tag{23b}$$

$$\text{NBC}: \quad \mathcal{I}(y;d_m,k_n) \approx \frac{1}{2\pi}\,\mathrm{e}^{\mathrm{i}k_n(z_l-y)\cdot d_m}\int_{S^1}\mathrm{e}^{\mathrm{i}k_n(y-z_l)\cdot\hat{x}}\rho^2\big(|B_l|+\hat{x}\cdot\mathbb{M}^0_{B_l}d_m\big)\,\mathrm{d}s(\hat{x}), \tag{23c}$$

the remainder term being small when $k\rho$ is small and $|\log k|\ll|\log\rho|$, which is the case for the frequency bands considered in the numerical examples below.

An interesting observation is that $\mathcal{I}(y;d_m,k_n)$ is just the zeroth-order Fourier coefficient of the renormalized field pattern $u_\rho^\infty(\,\cdot\,;d_m,k_n)$ after shifting the origin of the coordinate system to y (cf, e.g., Kress and Rundell [28, p 78]). This means that $\mathcal{I}(\,\cdot\,;d_m,k_n)$ processes only the low-frequency information contained in the far-field data and therefore should be relatively robust against high-frequency perturbations (e.g., due to measurement errors) in these data. We note that Fourier expansions of far-field patterns in appropriately shifted coordinate systems have been successfully used earlier to reconstruct the support of scatterers from far-field measurements of scattered fields (see, e.g., Sylvester *et al* [18, 29, 30, 36]).

The integrals in (23) can be evaluated explicitly using the following lemma:

Lemma 4.1. *Let $\xi,\,p\in\mathbb{R}^2$ and $k>0$. Then,*

$$\int_{S^1}\mathrm{e}^{-\mathrm{i}k\hat{x}\cdot\xi}\mathrm{d}s(\hat{x}) = 2\pi J_0(k|\xi|), \tag{24a}$$

$$\int_{S^1}\mathrm{e}^{-\mathrm{i}k\hat{x}\cdot\xi}\hat{x}\cdot p\,\mathrm{d}s(\hat{x}) = -2\pi\mathrm{i}\frac{\xi\cdot p}{|\xi|}J_1(k|\xi|). \tag{24b}$$

Proof. Working in polar coordinates we write $\xi = r_\xi(\cos\phi_\xi,\sin\phi_\xi)$, $\hat{x}=(\cos\theta,\sin\theta)$, and $p=r_p(\cos\phi_p,\sin\phi_p)$. Therewith,

$$\int_{S^1}\mathrm{e}^{-\mathrm{i}k\hat{x}\cdot\xi}\,\mathrm{d}s(\hat{x}) = \int_0^{2\pi}\mathrm{e}^{-\mathrm{i}kr_\xi\cos(\theta-\phi_\xi)}\,\mathrm{d}\theta = 2\int_0^\pi \mathrm{e}^{\mathrm{i}kr_\xi\cos\theta}\,\mathrm{d}\theta.$$

Recalling the integral representation of Bessel functions

$$J_n(\eta) = \frac{(-\mathrm{i})^n}{\pi}\int_0^\pi \mathrm{e}^{\mathrm{i}\eta\cos(\theta)}\cos(n\theta)\,\mathrm{d}\theta \tag{25}$$

(see, e.g., Abramowitz and Stegun [1, 9.1.21, p 360]) yields (24*a*).

Similarly,

$$\begin{aligned}\int_{S^1} \mathrm{e}^{-\mathrm{i}k\hat{x}\cdot\xi}\,\hat{x}\cdot p\,\mathrm{d}s(\hat{x}) &= \int_0^{2\pi} \mathrm{e}^{-\mathrm{i}kr_\xi\cos(\theta-\phi_\xi)} r_p\cos(\theta-\phi_p)\,\mathrm{d}\theta\\ &= \int_0^{2\pi} \mathrm{e}^{-\mathrm{i}kr_\xi\cos(\theta-\phi_\xi)} r_p\cos(\theta-\phi_\xi-(\phi_p-\phi_\xi))\,\mathrm{d}\theta\\ &= r_p\cos(\phi_p-\phi_\xi)\int_0^{2\pi} \mathrm{e}^{-\mathrm{i}kr_\xi\cos(\theta-\phi_\xi)}\cos(\theta-\phi_\xi)\,\mathrm{d}\theta\\ &= -2\frac{\xi\cdot p}{|\xi|}\int_0^{\pi} \mathrm{e}^{\mathrm{i}kr_\xi\cos\theta}\cos\theta\,\mathrm{d}\theta.\end{aligned}$$

Thus, (24*b*) follows from (25). □

Combining (23) and (24) we obtain that

$$\text{DBC}: \quad \mathcal{I}(y;d_m,k_n) \approx \sum_{l=1}^{L} \frac{1}{\log\rho}\,\mathrm{e}^{\mathrm{i}k_n d_m\cdot(z_l-y)} J_0(k_n|z_l-y|), \tag{26a}$$

$$\text{IBC}: \quad \mathcal{I}(y;d_m,k_n) \approx \sum_{l=1}^{L} \rho\overline{\lambda}_l|\partial B_l|\,\mathrm{e}^{\mathrm{i}k_n d_m\cdot(z_l-y)} J_0(k_n|z_l-y|), \tag{26b}$$

$$\begin{aligned}\text{NBC}: \quad \mathcal{I}(y;d_m,k_n) \approx \sum_{l=1}^{L} \rho^2\mathrm{e}^{\mathrm{i}k_n d_m\cdot(z_l-y)}\Big(&|B_l|J_0(k_n|z_l-y|)\\ &-\mathrm{i}\frac{z_l-y}{|z_l-y|}\cdot\mathbb{M}^0_{B_l} d_m J_1(k_n|z_l-y|)\Big).\end{aligned} \tag{26c}$$

To incorporate the multi-frequency information, we integrate $I(y;d_m,\cdot)$ numerically using all available wave numbers as in (21) and define for each incident direction $d_m\in S^1$,

$$\mathcal{I}_{\mathrm{MF}}(y;d_m) := \sum_{n=1}^{N} w_{k_n}\mathcal{I}(y;d_m,k_n), \tag{27}$$

where the weights are given by $w_{k_n} := (k_{n+1}-k_{n-1})/2$ for $n=2,\ldots,N-1$, $w_{k_1}=(k_2-k_1)/2$, and $w_{k_N}=(k_N-k_{N-1})/2$. The following lemma gives a theoretical motivation of this procedure.

Lemma 4.2. *Let $z,y\in\mathbb{R}^2$, $z\neq y$, and $d\in S^1$. Writing $p := d\cdot\frac{z-y}{|z-y|}$,*

$$\begin{aligned}\int_0^\infty \mathrm{e}^{\mathrm{i}kd\cdot(z-y)} J_0(k|z-y|)\,\mathrm{d}k &= \frac{1}{1-p}\frac{1}{|z-y|}, \qquad p\neq 1,\\ \int_0^\infty \mathrm{e}^{\mathrm{i}kd\cdot(z-y)} J_1(k|z-y|)\,\mathrm{d}k &= \frac{1}{|z-y|}+\mathrm{i}\frac{p}{(1-p)}\frac{1}{|z-y|}, \qquad p\neq 1.\end{aligned}$$

Proof. Let $a := |z-y|$ and $b := d\cdot(z-y)$. Then, $|b|\leqslant a$ and

$$a^2-b^2 = |z-y|^2\left(1-d\cdot\frac{z-y}{|z-y|}\right)^2 = |z-y|^2(1-p)^2.$$

Applying [1, 11.4.39, p 487] yields that

$$\int_0^\infty \mathrm{e}^{\mathrm{i}kd\cdot(z-y)} J_0(k|z-y|) = \frac{1}{\sqrt{a^2-b^2}}, \qquad |b|<a,$$

and similarly, using [1, 11.4.37, 11.4.38, p 487],

$$\int_0^\infty \mathrm{e}^{\mathrm{i}kd\cdot(z-y)} J_1(k|z-y|) = \frac{1}{a} + \mathrm{i}\frac{b}{a}\frac{1}{\sqrt{a^2-b^2}}, \qquad |b| < a.$$

This implies the desired results. □

So, considering $\mathcal{I}_{\mathrm{MF}}(y; d_m)$ from (27) as a (rough) approximation of $\int_0^\infty \mathcal{I}(y; d_m, k)\,\mathrm{d}k$, lemma 4.2 suggests that

$$\text{DBC}: \quad \mathcal{I}_{\mathrm{MF}}(y; d_m) \approx \sum_{l=1}^{L} \frac{1}{\log\rho}\frac{1}{1-p_{l,m}}\frac{1}{|z_l - y|}, \tag{28a}$$

$$\text{IBC}: \quad \mathcal{I}_{\mathrm{MF}}(y; d_m) \approx \sum_{l=1}^{L} \rho\overline{\lambda_l}|\partial B_l|\frac{1}{1-p_{l,m}}\frac{1}{|z_l - y|}, \tag{28b}$$

$$\text{NBC}: \quad \mathcal{I}_{\mathrm{MF}}(y; d_m) \approx \sum_{l=1}^{L} \rho^2\left(|B_l|\frac{1}{1-p_{l,m}} + \frac{z_l - y}{|z_l - y|}\cdot \mathbb{M}^0_{B_l} d_m\left(\frac{p_{l,m}}{1-p_{l,m}} - \mathrm{i}\right)\right)\frac{1}{|z_l - y|}, \tag{28c}$$

for $y \neq z_l$ and $p_{l,m} := d_m \cdot \frac{z_l - y}{|z_l - y|} \neq 1$, $1 \leqslant l \leqslant L$. Therefore, $\mathcal{I}_{\mathrm{MF}}(\,\cdot\,; d_m)$ is expected to have local maximums close to the position of the scatterers and to decay away from the scatterers, except along the lines $\{z_l - t d_m \mid t \geqslant 0\}$, where $p_{m,l} = 1$ and $\mathcal{I}_{\mathrm{MF}}(\,\cdot\,; d_m)$ might be large as well.

Integrating $\mathcal{I}_{\mathrm{MF}}(y; d_m)$ numerically over all available incident directions $d_1, \ldots, d_M$ will reduce the artifacts along the lines $\{z_l - t d_m \mid t \geqslant 0\}$. Therefore, we define the indicator function

$$\mathcal{J}(y) := \left|\sum_{m=1}^{M} w_{d_m} \mathcal{I}_{\mathrm{MF}}(y; d_m)\right|, \qquad y \in \mathbb{R}^2, \tag{29}$$

where the weight functions are chosen according to the composite trapezoid rule on S^1 with nodes $d_1, \ldots, d_M$. Then $\mathcal{J}$ should have distinct maximums close to the positions of the scatterers.

Remark 4.3. Since the positions of the scatterers z_l, $1 \leqslant l \leqslant L$, are unknown and $y \in \mathbb{R}^2$ varies, a particularly clever choice of the nodes $k_1, \ldots, k_N$ in the quadrature rule (27) to get an optimal approximation in (28) in the sense of lemma 4.2 is not available. However, numerical experiments confirm that already with relatively few evenly spaced wave numbers the finite sum $\mathcal{I}_{\mathrm{MF}}$ behaves qualitatively like the right-hand side of (28).

To exemplify this, we visualize in figure 1 the absolute values of the approximations

$$\sum_{k=1}^{N} w_k J_0(k|z-y|) \approx \int_0^\infty J_0(k|z-y|)\,\mathrm{d}k = \frac{1}{|z-y|}, \quad z \neq y, \tag{30a}$$

$$\sum_{k=1}^{N} w_k\, \mathrm{e}^{-\mathrm{i}k|z-y|} J_0(k|z-y|) \approx \int_0^\infty \mathrm{e}^{-\mathrm{i}k|z-y|} J_0(k|z-y|)\,\mathrm{d}k = \frac{1}{2|z-y|}, \quad z \neq y, \tag{30b}$$

$$\sum_{k=1}^{N} w_k J_1(k|z-y|) \approx \int_0^\infty J_1(k|z-y|)\,\mathrm{d}k = \frac{1}{|z-y|}, \quad z \neq y, \tag{30c}$$

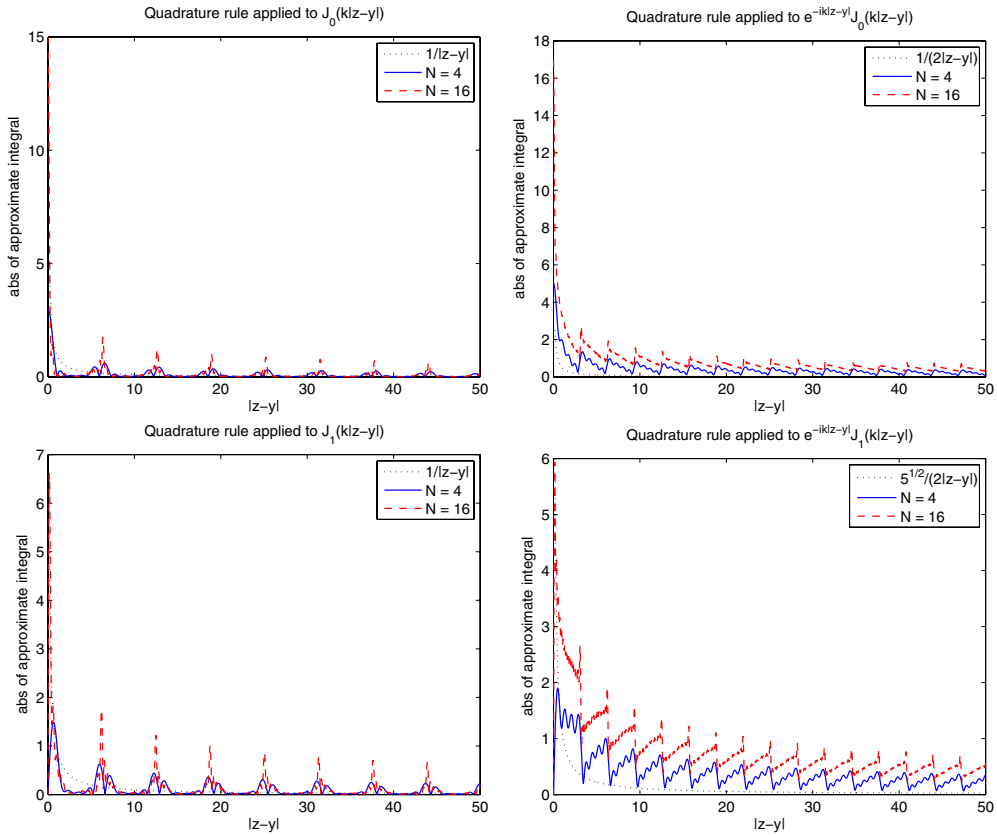

Figure 1. Rough approximations of the absolute values of the integrals in (30*a*) (top left), (30*b*) (top right), (30*c*) (bottom left), and (30*d*) (bottom right) for $N = 4$ and $N = 16$.

$$\sum_{k=1}^{N} w_k \mathrm{e}^{-\mathrm{i}k|z-y|} J_1(k|z-y|) \approx \int_0^\infty \mathrm{e}^{-\mathrm{i}k|z-y|} J_1(k|z-y|)\,\mathrm{d}k = \left(1 - \mathrm{i}\frac{1}{2}\right) \frac{1}{|z-y|}, \quad z \neq y, \tag{30d}$$

with weights w_k as in (27) for $N = 4$ and $N = 16$.

This corresponds to $p = 0$ and $p = -1$ in lemma 4.2. ⋄

5. Numerical results

In the following examples we study the behavior of the indicator function $\mathcal{J}$ from (29) numerically.

Example 5.1. First we consider a collection of four small elliptical scatterers with semi-axes of length 0.1 and 0.2 as shown in figure 2 (top left) and simulate far-field patterns corresponding to 16 incident plane waves with incident directions $d = (1, 0)$, $(0, 1)$, $(-1, 0)$, and $d = (0, -1)$ and wave numbers $k = 1, 2, 3$, and $k = 4$. This is performed for sound soft

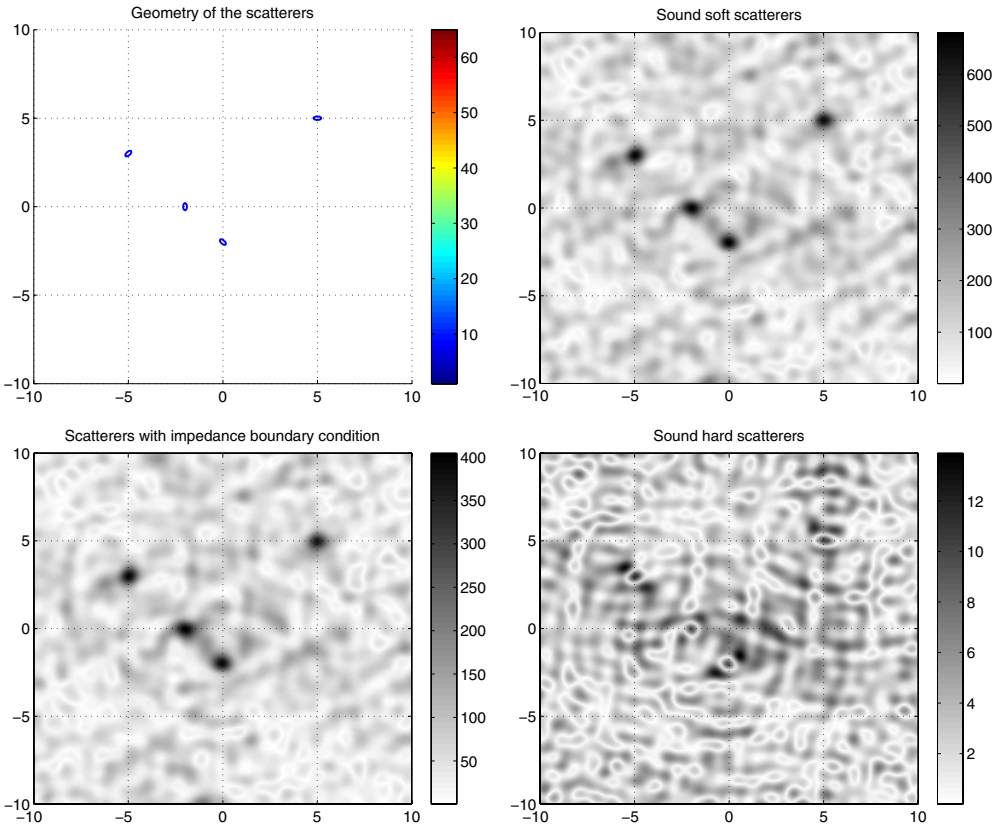

Figure 2. Geometrical setup of four scatterers (top left) and reconstructions of the scatterers with Dirichlet boundary conditions (top right), impedance boundary conditions (bottom left), and Neumann boundary conditions (bottom right) from simulated data without noise.

scatterers, sound hard scatterers, and for scatterers carrying an impedance boundary condition with surface impedance $\lambda = 0.5$ using the Nyström method described in [13, pp 67–72] and in [27] by Kress. We evaluate the far-field patterns at 32 equidistant points on the unit sphere S^1 and approximate the integral in (22) using the composite trapezoid rule.

Figure 2 shows visualizations of $\mathcal{J}$ for the three different boundary conditions. For sound-soft scatterers (top right) as well as for scatterers with impedance boundary conditions (bottom left) the position of the scatterers is nicely reconstructed. For sound-hard scatterers (bottom right) the quality of the reconstruction is worse but still the indicator function has local maximums at the position of the scatterers.

To show the versatility of the method also for sound-hard scatterers we include another example with more data corresponding to slightly higher wave numbers. Figure 3 (left) shows the reconstruction obtained with 32 incident plane waves corresponding to four incident directions as above, and eight wave numbers $k = 3, 4, 5, 6, 7, 8, 9$, and $k = 10$. The position of the scatterers is nicely reconstructed. Note that the resolution of the reconstructions increases as well.

Recalling (26) and lemma 4.2, the inferior performance of the reconstruction method for sound hard scatterers might be explained by the larger error of the quadrature rule (27) when applied to terms containing J_1, which has been exemplified in figure 1 (bottom row). Observing

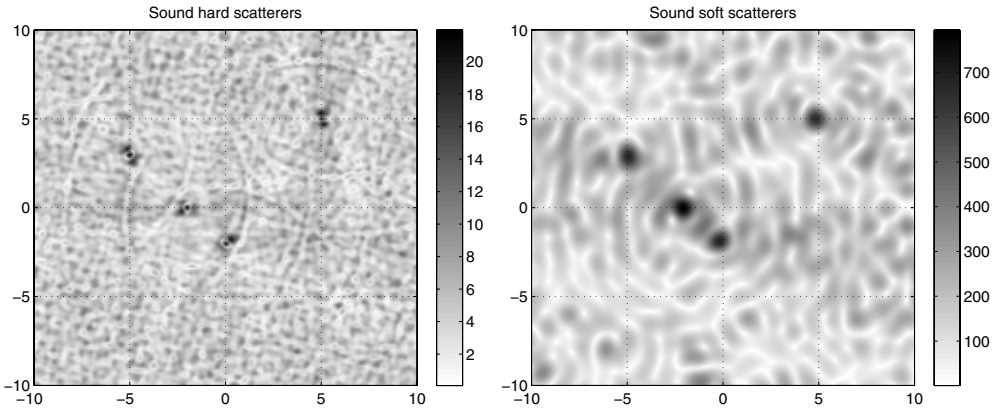

Figure 3. Reconstruction of four scatterers with Neumann boundary conditions using four incident directions and eight wave numbers (left) and reconstruction of four scatterers with Dirichlet boundary conditions using one incident direction and four wave numbers (right) from simulated data without noise.

that the first local maximum of $J_1(kr)$, $r \geqslant 0$, is at $r \approx 1.841/k$, while the first local maximum of $J_0(kr)$ is at $r = 0$, suggests that removing quadrature nodes at the lowest frequencies and adding nodes at higher frequencies, as performed in the previous reconstruction, improves the quality of approximation (27) in this case. This has indeed be confirmed by numerical experiments as in remark 4.3 not shown here.

If we reduce the number of incident directions and consider only four incident fields with a single incident direction $d = (1, 0)$ and wave numbers $k = 1, 2, 3$ and $k = 4$, the quality of the reconstruction decreases as well, as can be seen for sound soft scatterers in figure 3 (right). However, still this reconstruction is excellent.

To study the sensitivity of the algorithm against noise, we repeat the first experiment for sound soft scatterers with four incident directions and four different wave numbers, but now we add 25% and 75% uniformly distributed relative random error to the simulated far-field patterns before we start the reconstruction algorithm. As mentioned before, the values of the indicator function are essentially the sum of zeroth-order Fourier coefficients of the far-field patterns in appropriately translated coordinate systems. Thus, the method is expected to be relatively robust against high frequent random noise. The corresponding visualizations of $\mathcal{J}$ shown in figure 4 confirm this.

Example 5.2. In our second example we double the number of scatterers and consider a collection of eight small ellipses with semi-axes of length 0.1 and 0.2 as shown in figure 5 (top left). As in the previous example we start by using 16 incident plane waves with incident directions $d = (1, 0)$, $(0, 1)$, $(-1, 0)$, and $d = (0, -1)$ and wave numbers $k = 1, 2, 3$, and $k = 4$. We simulate the scattered field and evaluate its far-field pattern at 32 equidistant points on the unit sphere S^1. The reconstructions for sound soft scatterers (figure 5 top right) and scatterers carrying an impedance boundary condition with surface impedance $\lambda = 0.5$ (bottom left) are still good. However, in the case of sound hard scatterers (bottom right) the number and the position of the objects can hardly be estimated from this visualization of $\mathcal{J}$. If we increase the number of incident waves by adding higher frequencies and removing the two lowest frequencies the quality of the reconstruction improves. Figure 6 shows the corresponding results for sound hard scatterers with 32 incident fields with wave numbers

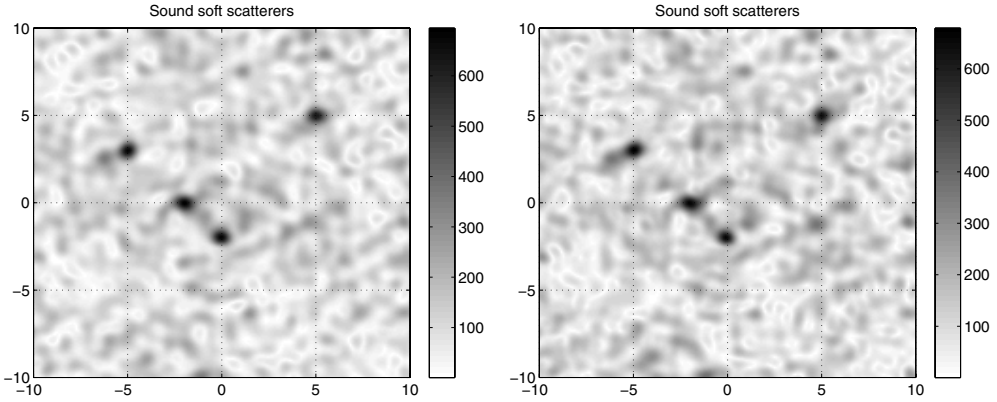

Figure 4. Reconstructions of four scatterers with Dirichlet boundary conditions from simulated noisy data containing 25% uniformly distributed relative error (left) and 75% uniformly distributed relative error (right).

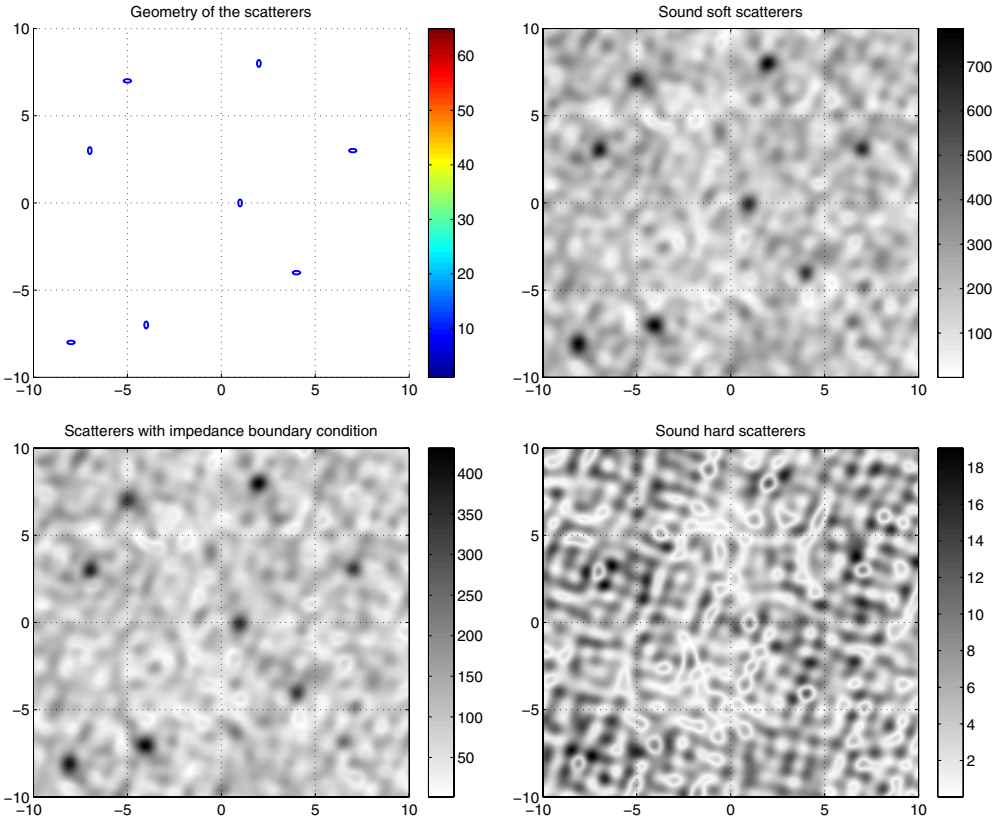

Figure 5. Geometrical setup of eight scatterers (top left) and reconstructions of the scatterers with Dirichlet boundary conditions (top right), impedance boundary conditions (bottom left), and Neumann boundary conditions (bottom right) from simulated data without noise.

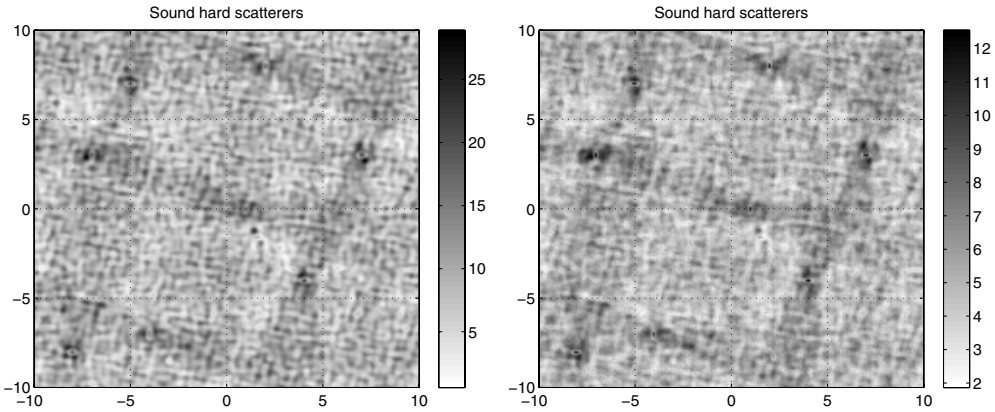

Figure 6. Reconstructions of eight scatterers with Neumann boundary conditions using four incident directions and eight wave numbers (left) and using four incident directions 16 wave numbers (right) from simulated data without noise.

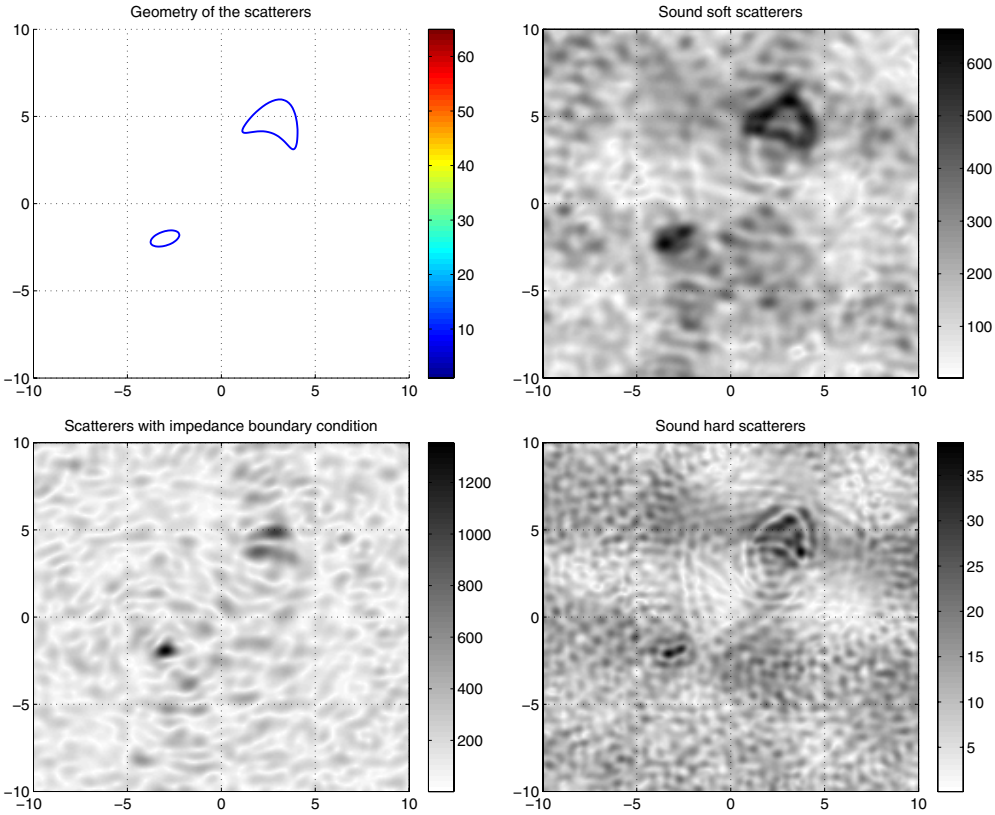

Figure 7. Geometrical setup of two extended scatterers (top left) and reconstructions of the scatterers with Dirichlet boundary conditions (top right), impedance boundary conditions (bottom left), and Neumann boundary conditions (bottom right) using four incident directions and four wave numbers from simulated data without noise.

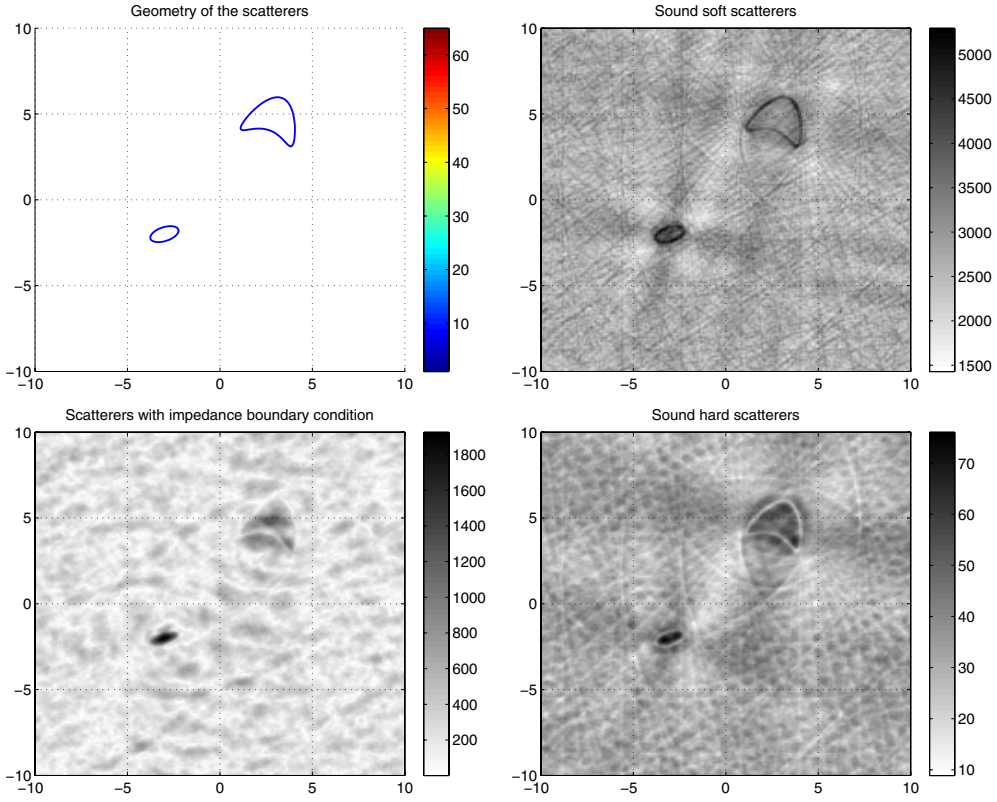

Figure 8. Geometrical setup of two extended scatterers (top left) and reconstructions of the scatterers with Dirichlet boundary conditions (top right), impedance boundary conditions (bottom left), and Neumann boundary conditions (bottom right) using four incident directions and 16 wave numbers from simulated data without noise.

$k = 3, \ldots, 10$ (left) and 64 incident fields with wave numbers $k = 3, \ldots, 18$. Six scatterers appear as distinct local maximums of the indicator function in the first plot, and all scatterers are reconstructed in the second plot.

Example 5.3. Since this paper has been motivated by the article [33], where the orthogonality sampling method was discussed in the resonance region, where the size of the scatterers is of the same order as the wave lengths of the incident fields we apply in our final example the modified orthogonality sampling algorithm developed in section 4 to reconstruct two extended scatterers as shown in figure 7 (top left).

The reconstructions obtained using 16 incident plane waves with incident directions $d = (1, 0)$, $(0, 1)$, $(-1, 0)$, and $d = (0, -1)$ and wave numbers $k = 1$, 2, 3, and $k = 4$ for sound soft scatterers and scatterers carrying an impedance boundary condition with surface impedance $\lambda = 0.5$ are shown in figure 7. For sound hard scatterers we use higher wave numbers $k = 3$, 4, 5, and $k = 6$ because lower frequencies tend to corrupt the reconstructions for this boundary condition as has already been observed in the previous examples. Again we use 32 evaluations of each far-field pattern on equidistant points on the unit sphere to approximate the integral in (22) using the composite trapezoid rule. As in the previous examples the results are best for sound soft scatterers (top right). For scatterers with impedance

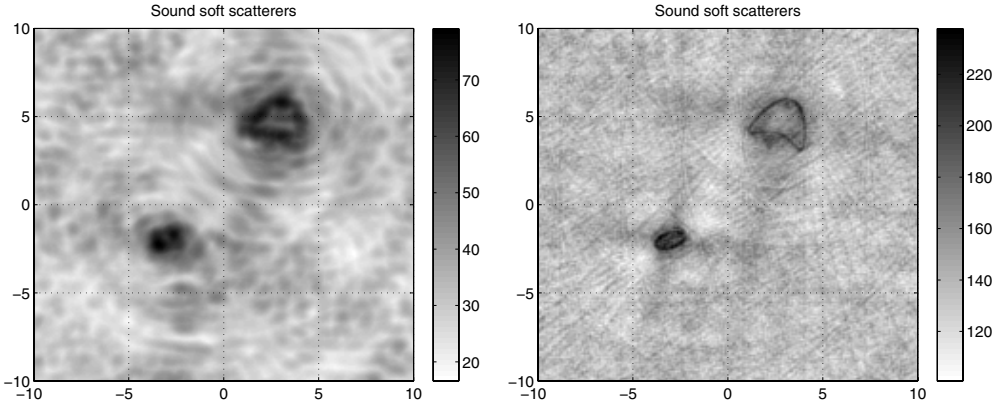

Figure 9. Reconstructions of the two extended scatterers with Dirichlet boundary conditions using the original orthogonality sampling algorithm by Potthast from [33] with four incident directions and four wave numbers (left) and 16 wave numbers (right) from simulated data without noise.

boundary conditions (bottom left) and sound hard scatterers (bottom right) the reconstructions are worse but still the number and the approximate positions of the scatterers can be estimated. Note that the boundary curves of the scatterers have not been plotted in these and the following plots: the exact values of $\mathcal{J}$ are seen.

Adding far-field patterns corresponding to incident waves with higher frequencies improves the reconstructions. Visualizations of $\mathcal{J}$ obtained using 64 incident plane waves with incident directions $d = (1, 0)$, $(0, 1)$, $(-1, 0)$, and $d = (0, -1)$ and wave numbers $k = 1, \ldots, 16$ for sound soft scatterers as well as for scatterers with the impedance boundary condition, and $k = 3, \ldots, 18$ for sound hard scatterers are shown in figure 8. The reconstructions are remarkably good. For sound soft scatterers the indicator function $\mathcal{J}$ has its maximum values exactly on the boundary of the scatterers. For scatterers carrying the impedance boundary condition and for sound hard scatterers the values of $\mathcal{J}$ are larger inside the obstacles than outside and they are close to zero on the boundaries of the scatterers. The artifacts away from the scatterers in opposite direction of the incident fields seen for sound soft and sound hard scatterers are in agreement with our remarks after (28).

Finally, we compare the results obtained with the modified orthogonality sampling algorithm developed in section 4 to reconstructions obtained with the original method from [33]. Figure 9 shows visualizations of $\Im$ from (21) for sound hard scatterers using 16 incident plane waves with incident directions $d = (1, 0)$, $(0, 1)$, $(-1, 0)$, and $d = (0, -1)$ and wave numbers $k = 1, 2, 3$, and $k = 4$ (*left*) and using 64 incident plane waves with incident directions $d = (1, 0)$, $(0, 1)$, $(-1, 0)$, and $d = (0, -1)$ and wave numbers $k = 1, \ldots, 16$ (right). We use 32 evaluations of each far-field pattern on equidistant points on the unit sphere to approximate the integral in (21) using the composite trapezoid rule. Comparing those with the plots in figure 7 (top right) and in figure 8 (top right) one could argue that the modified algorithm gives slightly cleaner reconstructions.

6. Concluding remarks

We discussed a simple non-iterative reconstruction method for inverse obstacle scattering problems for time-harmonic acoustic or electromagnetic waves that uses plane-wave incident fields with few incident directions but several wave numbers. Based on the assumption that the scatterers are small with respect to the wave lengths of the incident fields, we analyzed

the behavior of this method using an asymptotic expansion of the far-field patterns that holds across the corresponding frequency band. Numerical examples support our theoretical findings and suggest that the method works reasonably well also for inverse scattering in the resonance region, i.e. when the size of the scatterers is of the same order as the wavelength of the incident field. Clearly the main open problem is to give a theoretical justification of the multi-frequency orthogonality sampling algorithm in this case.

Comparing the orthogonality sampling method to MUSIC-type algorithms (see, e.g., [4, 10, 15, 25]), we observe that at each frequency orthogonality sampling requires far-field patterns corresponding to one or few incident waves only, i.e. one or a few columns of the so-called multi-static response matrix, while MUSIC processes the whole matrix at once. Using multiple frequencies, our numerical examples indicate that orthogonality sampling yields reconstructions of acceptable quality, being relatively robust against high-frequency noise in the measurement data. In this sense, orthogonality sampling is able to compensate a lack of incident directions of the incident waves by using multi-frequency information.

Acknowledgments

The author is pleased to thank Professor Martin Hanke–Bourgeois for many inspiring discussions on the topic of this work.

References

[1] Abramowitz M and Stegun I A (ed) 1966 *Handbook of Mathematical Functions, with Formulas, Graphs, and Mathematical Tables* (New York: Dover)
[2] Ammari H 2008 *An Introduction to Mathematics of Emerging Biomedical Imaging (Mathematics and Applications* vol 62*)* (Berlin: Springer)
[3] Ammari H, Griesmaier R and Hanke M 2007 Identification of small inhomogeneities: asymptotic factorization *Math. Comput.* **76** 1425–48
[4] Ammari H, Iakovleva E and Lesselier D 2005 Two numerical methods for recovering small electromagnetic inclusions from scattering amplitude at a fixed frequency *SIAM J. Sci. Comput.* **27** 130–58
[5] Ammari H, Iakovleva E and Moskow S 2003 Recovery of small inhomogeneities from the scattering amplitude at a fixed frequency *SIAM J. Math. Anal.* **34** 882–900
[6] Ammari H and Kang H 2004 *Reconstruction of Small Inhomogeneities from Boundary Measurements (Lecture Notes in Math.* vol 1846*)* (Berlin: Springer)
[7] Ammari H and Kang H 2004 Boundary layer techniques for solving the Helmholtz equation in the presence of small inhomogeneities *J. Math. Anal. Appl.* **296** 190–208
[8] Burkard C and Potthast R 2009 A time-domain probe method for three-dimensional rough surface reconstructions *Inverse Probl. Imaging* **3** 259–74
[9] Chen Q, Haddar H, Lechleiter A and Monk P 2010 A sampling method for inverse scattering in the time domain *Inverse Problems* **26** 085001
[10] Cheney M 2001 The linear sampling method and the MUSIC algorithm *Inverse Problems* **17** 591–5
[11] Colton D and Kirsch A 1996 A simple method for solving inverse scattering problems in the resonance region *Inverse Problems* **12** 383–93
[12] Colton D and Kress R 1983 *Integral Equation Methods in Scattering Theory* (New York: Wiley)
[13] Colton D and Kress R 1998 *Inverse Acoustic and Electromagnetic Scattering Theory (Appl. Math. Sci.* vol 93*)* 2nd edn (Berlin: Springer)
[14] Daido Y, Kang H and Nakamura G 2007 A probe method for the inverse boundary value problem of non-stationary heat equations *Inverse Problems* **23** 1787–800
[15] Devaney A J 1999 Super–resolution processing of multi-static data using time reversal and MUSIC (Boston, MA: Department of Electrical Engineering, Northeastern University) (preprint)
[16] Griesmaier R 2008 An asymptotic factorization method for inverse electromagnetic scattering in layered media *SIAM J. Appl. Math.* **68** 1378–403
[17] Guzina B B, Cakoni F and Bellis C 2010 On the multi-frequency obstacle reconstruction via the linear sampling method *Inverse Problems* **26** 125005

[18] Haddar H, Kusiak S and Sylvester J 2005 The convex back-scattering support *SIAM J. Appl. Math.* **66** 591–615
[19] Hansen D J and Vogelius M S 2008 High frequency perturbation formulas for the effect of small inhomogeneities *Proc. of 6th ICIPE, J. Phys.: Conf. Ser.* **135** 012106
[20] Ikehata M 2004 Inverse scattering problems and the enclosure method *Inverse Problems* **20** 533–51
[21] Ikehata M 2010 The enclosure method for inverse obstacle scattering problems with dynamical data over a finite time interval *Inverse Problems* **26** 055010
[22] Il'in A M 1992 *Matching of Asymptotic Expansions of Solutions of Boundary Value Problems (Translations of Mathematical Monographs* vol 102) translated by V Minachin (Providence, RI: American Mathematical Society)
[23] Jones D 1986 *Acoustic and Electromagnetic Waves (Oxford Science Publications)* (New York: Oxford University Press)
[24] Kirsch A 1998 Characterization of the shape of a scattering obstacle using the spectral data of the far-field operator *Inverse Problems* **14** 1489–512
[25] Kirsch A 2002 The MUSIC algorithm and the factorization method in inverse scattering theory for inhomogeneous media *Inverse Problems* **18** 1025–40
[26] Kress R 1989 *Linear Integral Equations (Appl. Math. Sci.* vol 82*)* (Berlin: Springer)
[27] Kress R 1995 On the numerical solution of a hypersingular integral equation in scattering theory *J. Comput. Appl. Math.* **61** 345–60
[28] Kress R and Rundell W 1997 Inverse obstacle scattering with modulus of the far-field pattern as data *Inverse Problems in Medical Imaging and Nondestructive Testing* ed H W Engl, A K Louis and W Rundell (Vienna: Springer)
[29] Kusiak S and Sylvester J 2003 The scattering support *Commun. Pure Appl. Math.* **56** 1525–48
[30] Kusiak S and Sylvester J 2005 The convex scattering support in a background medium *SIAM J. Math. Anal.* **36** 1142–58
[31] Luke D R 2004 Multifrequency inverse obstacle scattering: the point source method and generalized filtered backprojection *Math. Comput. Simul.* **66** 297–314
[32] Potthast R 2001 *Point Sources and Multipoles in Inverse Scattering Theory (CRC Research Notes in Mathematics)* (Boca Raton, FL: CRC)
[33] Potthast R 2010 A study on orthogonality sampling *Inverse Problems* **26** 074015
[34] Potthast R, Sylvester J and Kusiak S 2003 A 'range test' for determining scatterers with unknown physical properties *Inverse Problems* **19** 533–47
[35] Simonetti F and Huang L 2008 From beamforming to diffraction tomography *J. Appl. Phys.* **103** 103110
[36] Sylvester J 2006 Notions of support for far fields *Inverse Problems* **22** 1273–88
[37] Vänskä S 2008 Stationary waves method for inverse scattering problems *Inverse Probl. Imaging* **2** 577–86
[38] Vogelius M S and Volkov D 2000 Asymptotic formulas for perturbations in the electromagnetic fields due to the presence of inhomogeneities of small diameter *Math. Model. Numer. Anal.* **34** 723–48